Cite this : New Carbon Materials, 2023, 38(1): 143-153 **DOI:** 10.1016/S1872-5805(22)60615-2

Nitrogen doped hollow porous carbon fibers derived from polyacrylonitrile for Li-S batteries

NIU Jing-yi[1,2,4], JING De-qi[1,4], ZHANG Xing-hua[1,4], SU Wei-guo[3], ZHANG Shou-chun[1,2,4,*]

（1. *CAS Key Laboratory for Carbon Materials*, *Institute of Coal Chemistry*, *Chinese Academy of Sciences*, *Taiyuan* 030001, *China*;
2. *Center of Materials Science and Optoelectronics Engineering*, *University of Chinese Academy of Sciences*, *Beijing* 100049, *China*;
3. *National Key Laboratory of Science and Technology on Vessel Integrated Power System*, *Naval University of Engineering*, *Wuhan* 430033, *China*;
4. *National Engineering Laboratory for Carbon Fiber Technology*, *Institute of Coal Chemistry*, *Chinese Academy of Sciences*, *Taiyuan* 030001, *China*）

Abstract: Hollow porous carbon fibers for Li-S battery electrodes were prepared by the KOH activation of carbon prepared from hollow polyacrylonitrile fibers. The fibers had a high specific surface area of 2 491 $m^2 \cdot g^{-1}$, a large pore volume of 1.22 $cm^3 \cdot g^{-1}$ and an initial specific capacity of 330 $mAh \cdot g^{-1}$ at a current density of 1 C. To improve their electrochemical performance, the fibers were modified by treatment with hydrazine hydrate to prepare nitrogen-doped hollow porous carbon fibers with a specific surface area of 1 690 $m^2 \cdot g^{-1}$, a pore volume of 0.84 $cm^3 \cdot g^{-1}$ and a high nitrogen content of 8.81 at%. Because of the increased polarity and adsorption capacity produced by the nitrogen doping, the initial specific capacity of the fibers was increased to 420 $mAh \cdot g^{-1}$ at a current density of 1 C.

Key words: Hollow-shaped carbon fibers; Activation; Modification; Li-S batteries

1 Introduction

In the past few decades, lithium-ion batteries (LIBs) have occupied the new energy market because of their long cycling stability, high energy density, high operating voltage and Coulombic efficiency[1, 2]. However, the current systems of LIBs cannot keep up with the increasing performance demanded by electronic vehicles[1, 3]. Inspired by the rising demand for sophisticated energy storage systems, lithium-sulfur (Li-S) batteries came to be regarded as the most promising next-generation high-performance energy storage system. The Li-S batteries have higher theoretical specific capacity of 1 675 $mAh \cdot g^{-1}$ and energy density of 2 600 $Wh \cdot kg^{-1}$[4–6]; several times higher than LIBs. In addition, compared with conditional cathode materials, monomeric sulfur is resource-rich, environment-friendly, inexpensive, and easily available[7].

The charge and discharge process of the Li-S batteries is realized by the transport of lithium ions between the two electrodes[8]. During the initial discharge, the active material sulfur exists in the form of cyclic molecules. As the voltage drops, the sulfur-sulfur bonds (S-S) of the cyclic molecules are broken, generating long-chain polysulfides (Li_2S_n, $4<n\leqslant 8$). As the reaction proceeds, these are reduced to short-chain polysulfides (Li_2S_n, $2<n\leqslant 4$), which are finally reduced to lithium sulfide (Li_2S)[8–10]. The multi-electron reaction of sulfur phase transition gives Li-S batteries good electrochemical performance, but some problems arise. The main problem is the “shuttle effect” of polysulfide ions (Li_2S_n, $2<n\leqslant 8$), which are easily dissolved during cycling, leading to the low actual specific capacity and fast decay at high rates[11]. On the other hand, the insulating properties of sulfur and insoluble Li_2S_2/Li_2S reduce utilization of the active substances. Due to densities of sulfur and Li_2S being 2.03 and 1.66 $g \cdot cm^{-3}$, respectively, volume expansion occurs during the cycle. In addition, there are problems such as “lithium dendrites”, solid electrolyte interphase (SEI) and self-discharge[5, 7, 10–13]. These effects cascade down to bigger problems like severe capacity degradation, low Coulombic efficiency and insufficient cycle life.

Great efforts have been made to solve these problems, especially focusing on the preparation of better cathode materials[14]. Limiting “shuttle effect” of polysulfides by physical confinement and chemical bond-

Received date: 2022-04-06; **Revised date:** 2022-05-10
Corresponding author: ZHANG Shou-chun, Professor. E-mail: zschun@sxicc.ac.cn
Author introduction: NIU Jing-yi, Master. E-mail: niujingyii@163.com

ing are commonly used methods. In addition, the ideal anode structure should have the following properties: a substrate with good mechanical properties to prevent structural damage; enough space to cushion volume expansion; a large conductive matrix to accelerate electron/ion transfer, and larger specific surface area to contain sulfur[10].

Numerous studies have shown that carbonaceous materials are excellent hosts of sulfur[15], such as carbon nanotubes[16], graphene foam[3], metallic MoS_2 nanoflowers decorated graphene nanosheet[14], N-doped porous carbon cages[17], free-standing carbon nanofibers interlayer[18], activated carbon fiber cloth[19] and so on. The hollow carbon nanofiber arrays were synthesized by Zheng et al.[10] using the anodized aluminum template method (AAO). The specific capacity of 730 $mAh \cdot g^{-1}$ was obtained by charging and discharging 150 times at 0.2 C, which illustrated that the high aspect ratio of the carbon nanofibers were ideal structures for this purpose. You et al.[4] fabricated a-MEGO/S composite by using microwave exfoliation of graphite oxide and KOH activation. A hierarchically micro/mesoporous a-MEGO with higher specific surface area (3 000 $m^2 \cdot g^{-1}$) and pore volume (2.14 $cm^3 \cdot g^{-1}$) was utilized, which proved that materials with high specific surface area and large pore volume were suitable sulfur host materials. Zhang et al.[20] designed a lotus root-like carbon fiber modified by CoS_2. The integrated electrodes achieved high capacity of 1 015 $mAh \cdot g^{-1}$ at 0.2 $A \cdot g^{-1}$, which showed that modification by transition metal compounds can improve electrochemical performance.

Hollow-shaped carbon fiber has good electrical conductivity and unique cavity structure. By treatment, it is easy to increase its specific surface area, and modify various other properties. Herein, N-doped hollow-shaped porous PAN-CFs with high specific surface area were utilized in Li-S batteries. Using PAN hollow-shaped fiber as the precursor, hollow-shaped porous carbon fibers activated by KOH at 800 °C exhibited higher specific surface area of 2 491 $m^2 \cdot g^{-1}$, larger pore volume of 1.22 $cm^3 \cdot g^{-1}$, good conductive network and hierarchical porous structure. Because of the high specific surface area, hollow-shaped CFs achieved high sulfur loading of 75 wt.%, obtaining initial specific capacity of 330 $mAh \cdot g^{-1}$ at 1 C rate. Meanwhile, the modification of carbon fibers with hydrazine hydrate increased its nitrogen content by 122.2%, with a nitrogen content as high as 8.81 at%. When the nitrogen doped hollow-shaped porous carbon fiber was used as Li-S battery electrodes, its initial specific capacity increased to 420 $mAh \cdot g^{-1}$ at current density of 1 C, and the Coulombic efficiency was about 100%. This work provides a new idea for the application of carbon fibers as sulfur hosts in Li-S batteries.

2 Experimental

2.1 Materials

Potassium hydroxide (KOH), hydrochloric acid (HCl), hydrazine hydrate ($N_2H_4 \cdot H_2O$) and acetylene black were purchased from Sinopharm Chemical Reagent Co. Sulfur powder (900 mesh) was purchased from Alfa Aesar Chemical Co., Ltd. N-Methylpyrrolidone (NMP) and poly(1,1-difluoroethylene) (PVDF) were purchased from Aladdin. The hollow-shaped PAN precursor fibers filament was provided by the Institute of Coal Chemistry, Chinese Academy of Sciences.

2.2 Synthesis of N-doped hollow-shaped porous CFs

Firstly, hollow-shaped PAN precursor fiber was pre-oxidized in fluid air at 190, 220 and 250 °C for 2 h; then it was carbonized at 700 °C for 1 h. Secondly, the carbonized fibers were activated by KOH at 600, 700, 800 and 900 °C for 1 h (weight ratio of KOH∶CF=2∶1). The carbonation and activation process were carried out in a tube furnace with nitrogen as protective gas at a flow rate of 200 $mL \cdot min^{-1}$ and a heating rate of 10 $°C \cdot min^{-1}$. Finally, activated carbon fibers were washed with 1 $mol \cdot L^{-1}$ of hydrochloric acid and deionized water for neutralization. After drying in an oven at 60 °C, the obtained hollow-shaped porous carbon fiber was denoted as HSPCF-X (X=600, 700, 800, 900).

The PAN precursor fiber was pre-treated with hydrazine hydrate by heating and stirring at 95 °C for

20 h. After that, the fiber was washed with deionized water, and dried to a constant weight. Then, carbon fiber was pre-oxidized, carbonized and activated sequentially according to the same process conditions as described above. In this way, the nitrogen-enriched hollow-shaped porous carbon fiber could be obtained and marked as N-HSPCF.

2.3 Cell assembly

Porous carbon fiber was melted and blended with sulfur, kept at 155 °C for 12 h in N_2 to obtain carbon fiber/sulfur (CF/S) composites. A homogeneous slurry was fabricated by dissolving 80 wt.% CF/S composites, 10 wt.% acetylene black and 10 wt.% PVDF in NMP.

The slurry was evenly coated on the carbon-coated aluminum foil, and the solvent was evaporated overnight in a vacuum oven, then cut into circular electrodes from the as-obtained positive electrode material. Finally, the electrode material was loaded into CR2032 batteries in an argon-protected glove box.

2.4 Characterization

The morphology of the porous carbon fiber was characterized by scanning electron microscopy (SEM, JEOL 7900F) and transmission electron microscopy (TEM, JEM-2100F). Nitrogen adsorption-desorption isotherms and pore size distributions were analyzed with a nitrogen physisorption apparatus (ASAP 2020 HD88). The chemical composition of the fibers' surface was characterized by X-ray photoelectron spectroscopy (XPS). Thermogravimetric analysis (STA 449F3) was carried out at 25-600 °C in nitrogen atmosphere.

2.5 Electrochemical measurements

The cycle and rate capability were obtained by a LAND 3002A battery testing system. The cyclic voltammetry (CV) and electrochemical impedance spectroscopy (EIS) measurements were carried out on the CHI660E. The voltage range for CV testing was 1.7-2.8 V, and the EIS test was performed in the frequency range of 0.01 to 100 kHz.

3 Results and discussion

As seen from the SEM images of PAN hollow-shaped carbon fibers (HSPCF) (Fig.1), the surface of the fibre is relatively smooth devoid of any obvious groove structure after carbonization, which is inherited from the precursor of PAN fibers manufactured by dry-jet wet spinning. The outer diameter of hollow-shaped carbon fibers is approximately 25 μm (Fig. 1a). The SEM image in Fig. 1b is the cross-section of single carbon fiber, showing an internal cavity structure with a diameter of about 9 μm, which can provide a channel for sulfur loading and ion diffusion.

The pore structure analysis of the HSPCF-X is performed as shown in Fig. 2. HSPCF-600 and HSPCF-700 show predominantly type-I adsorption and de-

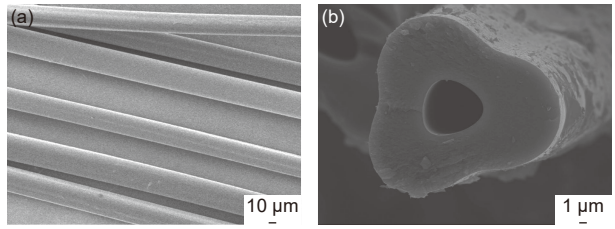

Fig. 1　SEM images of PAN hollow-shaped carbon fibers of (a) surface and (b) cross-section

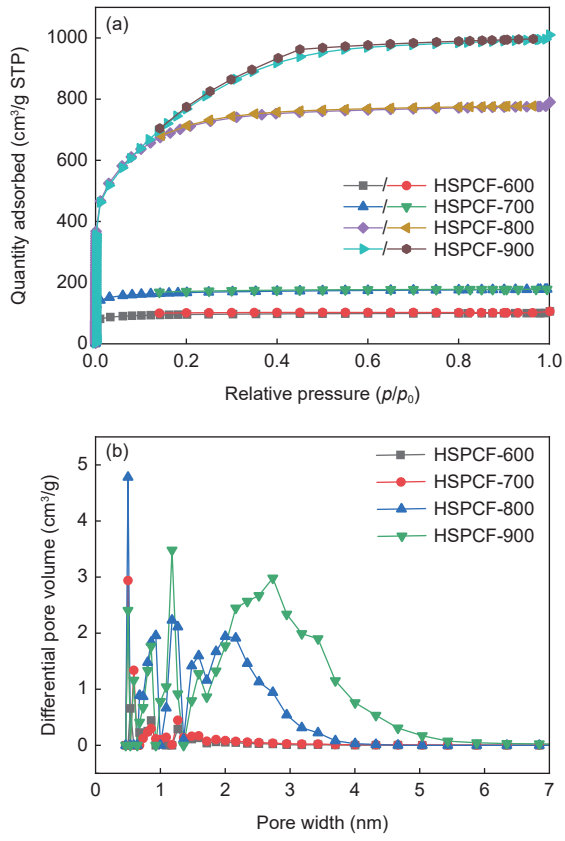

Fig. 2　(a) N_2 adsorption/desorption isotherms and (b) pore size distribution obtained from DFT method for HSPCF-X (X=600, 700, 800, 900)

sorption curve, indicating that HSPCF-600 and HSPCF-700 have a mostly microporous structure (Fig. 2a). HSPCF-800 and HSPCF-900 show combination of type I and type IV adsorption and desorption isotherms[21, 22], indicating that these two samples have a hierarchical pore structure. As shown in Fig. 2b, the peaks of HSPCF-600 and HSPCF-700 exist at 0.4, 0.6, 0.8 and 1.3 nm. Compared with HSPCF-600, HSPCF-700 has higher peaks at these four locations, which is due to the slow reaction at 600 °C. The degree of reaction between carbon and KOH becomes more intense with increasing temperature, and the pore structure becomes more developed. In addition to the pores with peaks at 0.4, 0.8 and 1.3 nm, HSPCF-800 and HSPCF-900 have a pore size distribution at the range of 1.4-3.7 nm and 1.4-5.5 nm, respectively. HSPCF-900 has larger pore volume (1.56 $cm^3 \cdot g^{-1}$) (Table 1), because with the increase of activation temperature, the reaction degree increases, the micropore wall collapses, the pore size increases and gradually develops into mesopores. In summary, in the range of 600-900 °C, the increase in temperature favors the activation reaction and the pore size and volume gradually increase.

The pore structure parameters of each sample are listed in Table 1. The specific surface area and pore volume of the HSPCF-X increases significantly compared with the untreated carbon fibers, and this increase is also correlated with the increase of temperature in the range of 600-900 °C. The micropore area shows a trend of increasing and then decreasing, up to 992.42 $m^2 \cdot g^{-1}$.

Fig. 3 shows the cycling performance curves of the composite electrodes of hollow porous carbon

Table 1 Pore structure parameters of samples

Sample	S_{BET}(m^2 g^{-1})	S_{micro}(m^2 g^{-1})	V_{total}(cm^3 g^{-1})	V_{BJH}(cm^3 g^{-1})
HSCF	0.19	-	-	-
HSPCF-600	323.31	260.19	0.16	0.021
HSPCF-700	566.05	449.23	0.28	0.045
HSPCF-800	2490.98	992.42	1.22	0.407
HSPCF-900	2813.15	95.90	1.56	1.131

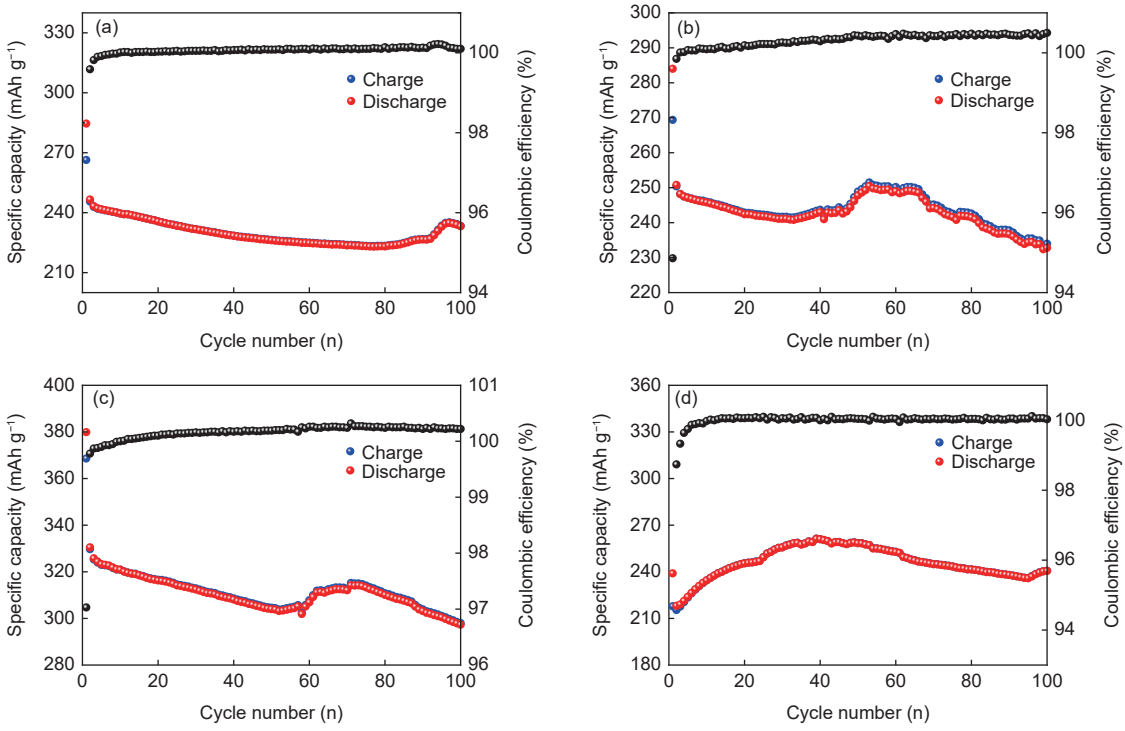

Fig. 3 Cycling performance curves of HSPCF-X/sulfur composite electrodes at current density of 1 C (1 C=1675 mA g^{-1}): (a) HSPCF-600, (b) HSPCF-700, (c) HSPCF-800 and (d) HSPCF-900

fiber and sulfur under different activation temperature conditions. After 100 cycles at 1 675 $mA \cdot g^{-1}$, Coulombic efficiencies are about 100 %, and the specific capacities of the materials obtained by activation treatment at 600, 700, 800 and 900 °C are 246, 252, 330 and 220 $mA \cdot g^{-1}$, respectively. The specific surface area of HSPCF-800 is not the highest, from which it can be concluded that when the carbon material is used as the substrate, beyond a certain extent, the increase in specific surface area does not necessarily improve the specific capacity. The four charging and discharging curves do not show a stable decaying trend, which may be due to insufficient activation of the cell or related to the change of ambient temperature during charging and discharging (Fig. 3a). In conclusion, the electrode obtained when activated at 800 °C has the highest specific capacity. Hereinafter, HSPCF is replaced by HSPCF-800.

Results from SEM, TEM and EDS were obtained to analyze the porous structure of the N-HSPCF. From Fig. 4a, the sample diameter is reduced to about 20 μm after the treatment of hydrazine hydrate, oxidation, carbonization and activation, and a clear groove structure appears on the fiber's surface (Fig. 4b). The TEM image clearly shows a distinct pore structure (Fig. 4c), which is formed due to the chemical reaction of KOH with carbon. Elemental mapping analysis (Fig. 4d,e) is carried out, where one can see that the nitrogen and carbon elements are mostly situated on the surface of the N-HSPCF. The results confirm that after treatment with hydrazine hydrate and activation, nitrogen atoms and pore structure are successfully introduced into the fibers.

The pore structure characteristics of the prepared porous carbon fibers (HSPCF and N-HSPCF) are demonstrated (Fig. 5). Clearly, HSPCF and N-HSPCF show a type Ⅰ+Ⅳ adsorption curve in Fig. 5a[23], the adsorption curves are approximately vertical in the low-pressure area, indicating the presence of massive micropores in HSPCF and N-HSPCF; while the small hysteresis loop suggests certain mesopores in them. This is because KOH reacts with carbon fibers during the activation process at 800 °C and generats a large number of micropores, some of which even develop into mesopores. The pore size distribution of HSPCF and N-HSPCF in Fig. 5b illustrate their micropores are mainly distributed at 0.80, 1.35 and 1.65 nm, meanwhile, there are a certain amount of mesopores at 2.0-3.5 nm. This is consistent with adsorption-desorption curves. Besides, the mesopores content of N-HSPCF is significantly less than that of N-HSPCF, which is caused by the secondary nitrogen enrichment treatment. From the pore structure parameters of HSPCF and N-HSPCF in Table 2, HSPCF has higher specific surface area of 2 491 $m^2 \cdot g^{-1}$ than N-HSPCF (1 690 $m^2 \cdot g^{-1}$).

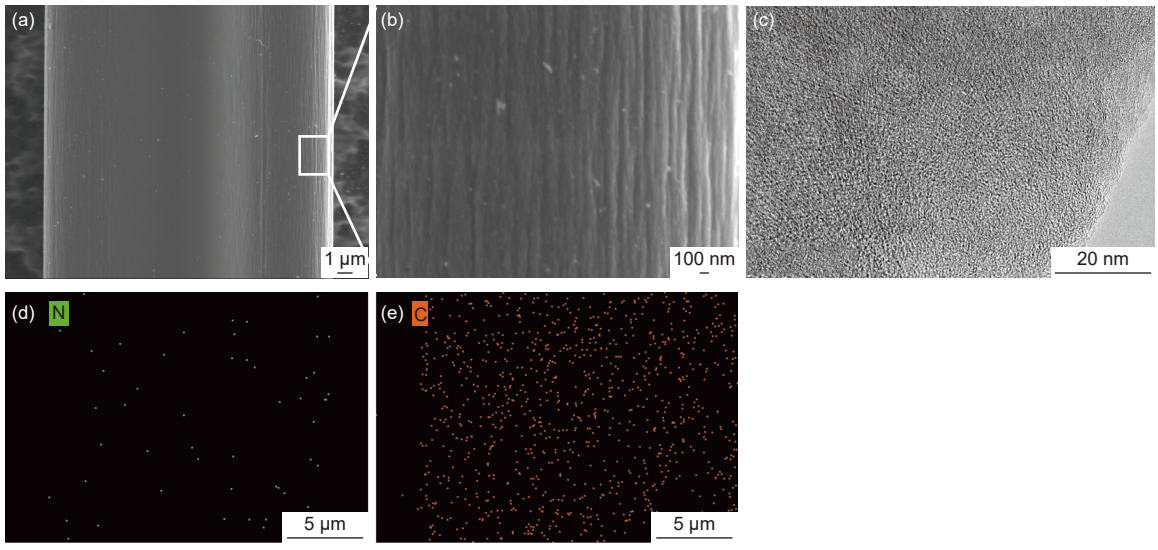

Fig. 4　(a) SEM image of the surface of N-HSPCF, (b) Magnification of the white rectangle region in (a). (c) TEM image of N-HSPCF. Elemental maps of (d) nitrogen and (e) carbon corresponding to (a)

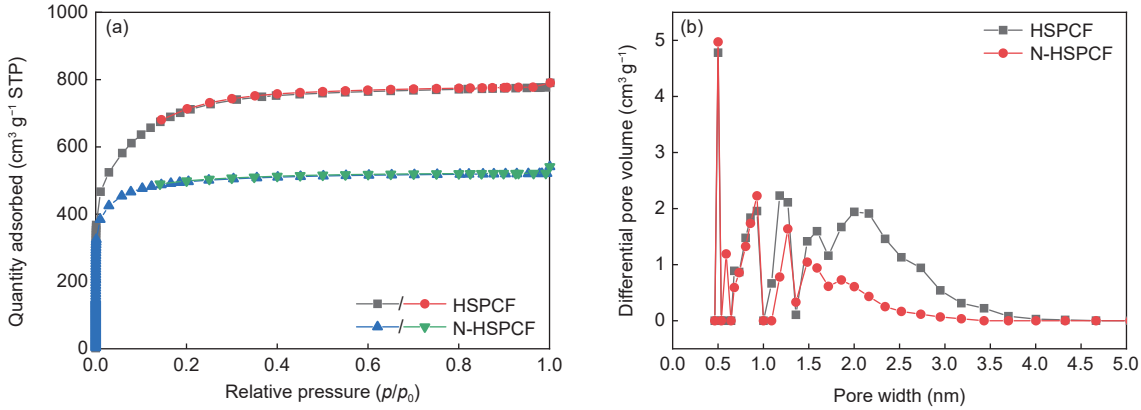

Fig. 5 (a) N_2 adsorption isotherms and (b) pore size distributions of HSPCF and N-HSPCF

Table 2 Pore structure parameters of HSPCF and N-HSPCF

Samples	S_{BET} ($m^2 \cdot g^{-1}$)	S_{micro} ($m^2 \cdot g^{-1}$)	V_{total} ($cm^3 \cdot g^{-1}$)	V_{BJH} ($cm^3 \cdot g^{-1}$)
HSPCF	2491	992	1.22	0.41
N-HSPCF	1690	1307	0.84	0.12

The possible reason for this difference is that after hydrazine hydrate treatment, the cross-linking reaction occurs between PAN molecules to form a three-dimensional network of cross-linked structure[24]. During the pre-oxidation process, due to the occurrence of cyclization and dehydrogenation reactions, small molecules are released, molecular chains are arranged more tightly, and the carbon skeleton shrinks. Following the carbonization process, the carbon skeleton shrinks more obviously after further dehydrogenation and cross-linking reactions.

Fig. 6a shows the morphology of the fibers blended with sulfur. The fiber still maintains the original morphology after blending. The element mapping of sulfur-loaded porous carbon fiber is shown in Fig. 6b, c. The sulfur is evenly distributed on the inner and outer surfaces of the hollow porous carbon fiber shell

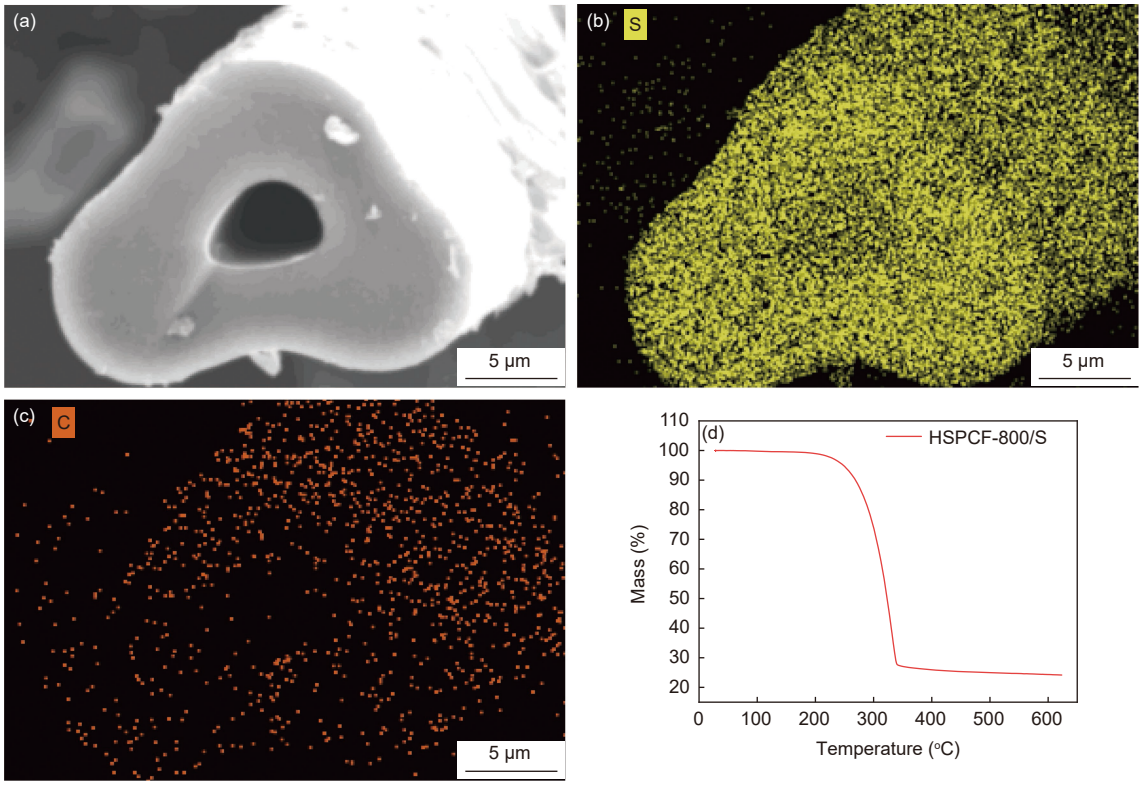

Fig. 6 (a) SEM image of CFs/S, elemental mapping of (b) sulfur, (c) carbon, (d) TG curve of CFs/S composite

wall, which also proves the existence of a large number of pore structures. At the same time, a thermogravimetric analysis of the CFs/sulfur composites is performed (Fig. 6d). It could be seen that a weight loss of 75 wt.% occurred during the heating process, indicating that the prepared composite material has high sulfur loading with a sulfur content of 75 wt.%.

Fig. 7a shows the XPS full spectra of HSPCF and N-HSPCF, the nitrogen content of HSPCF is 4.15 at%, while the nitrogen content of N-HSPCF after treatment with hydrazine hydrate is up to 8.81 at%. Generally, the nitrogen functional groups include pyridine nitrogen (N-P, 398.5 eV), hydroxy pyridine and pyrrole nitrogen (N-X, 400.3 eV), graphitized nitrogen (N-Q, 401.2 eV) and pyridine nitrogen oxide (N-O, 403-405 eV) as shown in Fig. 7b[15, 17, 24–26]. For HSPCF, the N1s spectrum can be divided into 3 peaks: N-X, N-Q and N-O, which account for 40.29%, 55.16% and 4.55%, respectively (Table 3). While for N-HSPCF, the N1s spectrum is fitted as N-P, N-X and N-Q, accounting for 19.25%, 53.50% and 26.75%, respectively. The differences in the types and contents of nitrogen-containing functional groups for HSPCF and N-HSPCF might be because hydrazine hydrate can cross-link with PAN branches and form new bonds[23, 27–28].

The CV and EIS tests are conducted to evaluate the performance of HSPCF/S and N-HSPCF/S electrodes. The CV test is carried out at potential window of 1.7-2.8 V. As shown in Fig. 8a, both curves have two obvious reduction peaks and an oxidation peak, which correspond to the reduction of sulfur to long-

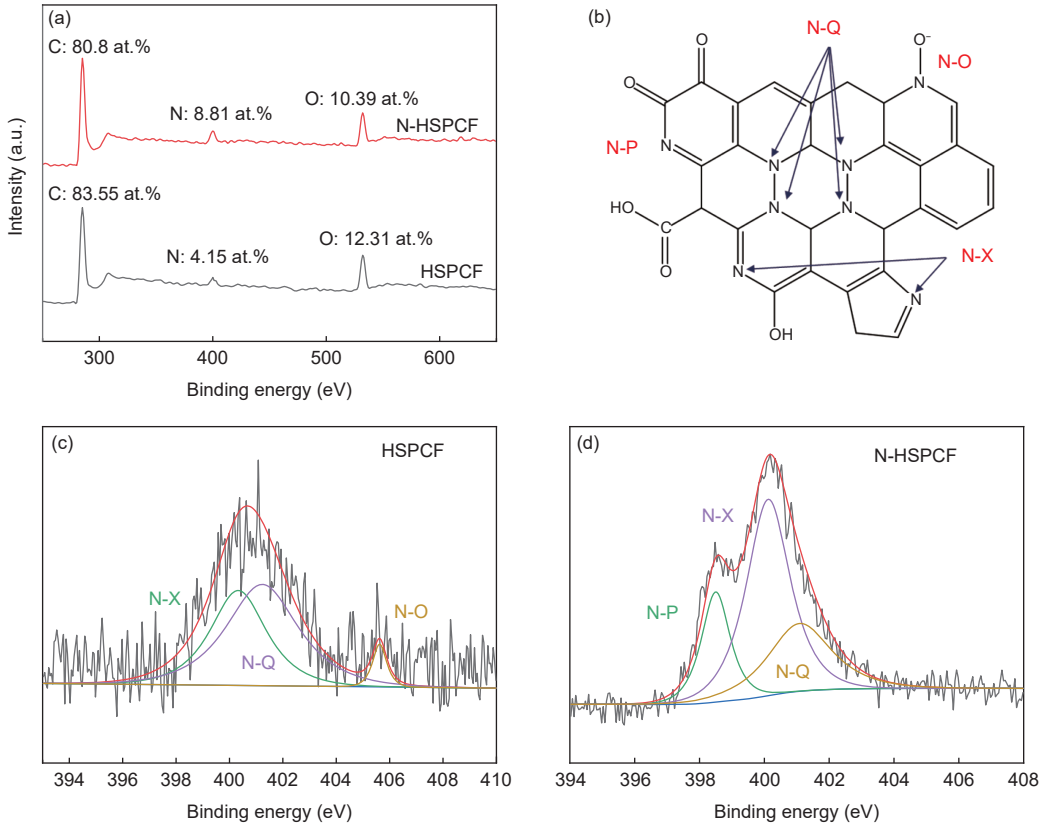

Fig. 7　(a) XPS full spectra of HSPCF and N-HSPCF. (b) Types of nitrogen-containing functional groups. N1s spectra of (c) HSPCF and (d) N-HSPCF

Table 3　The content of surface nitrogen-containing functional groups for HSPCF and N-HSPCF

Sample	XPS (at. %)			Nitrogen functional group (%)			
	C	N	O	N-P	N-X	N-Q	N-O
HSPCF	83.55	4.15	12.31	-	40.29	55.16	4.55
N-HSPCF	80.80	8.81	10.39	19.25	53.50	26.75	-

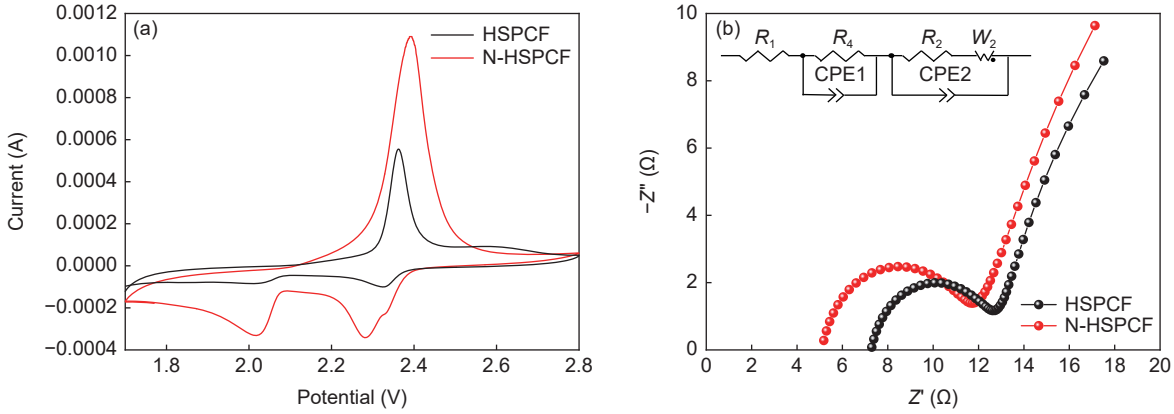

Fig. 8 (a) CV curves of cells with HSPCF/S electrodes and N-HSPCF/S electrodes at 0.15 mV·s^{-1}. (b) EIS spectra of cells with HSPCF/S electrodes and N-HSPCF/S electrodes from 0.01 to 100 kHz

chain polysulfides (Li_2S_x, $4 \leqslant x \leqslant 8$) around 2.3 V, and further reduction into short-chain polysulfides and insoluble Li_2S_2/Li_2S around 2.05 V[6]. N-HSPCF/S shows more intense redox peaks compared with HSPCF/S cells, indicating that the introduction of nitrogen-containing functional groups facilitates the conversion of polysulfide[29]. EIS is used to analyze the cell internal resistance and charge-transfer resistance of HSPCF and N-HSPCF[6] as shown in Fig. 8b. The Nyquist plots consist of a single semicircle in the high-to-medium frequency region and an arc in the low frequency region, which include charge-transfer resistance R_2 and a mass-transfer process[30]. After secondary nitrogen enrichment treatment, the value of R_2 decreases, which indicate that the N-HSPCF/S electrode has faster charge transfer process. Besides, the N-HSPCF/S electrode shows smaller internal resistance compared with the HSPCF/S electrode.

The cycle performance curves of HSPCF/S and N-HSPCF/S electrodes at 1 C rate are shown in Fig. 9. The initial specific capacity of HSPCF (Fig. 9a) is only 330 mAh·g^{-1}, and the initial specific capacity of

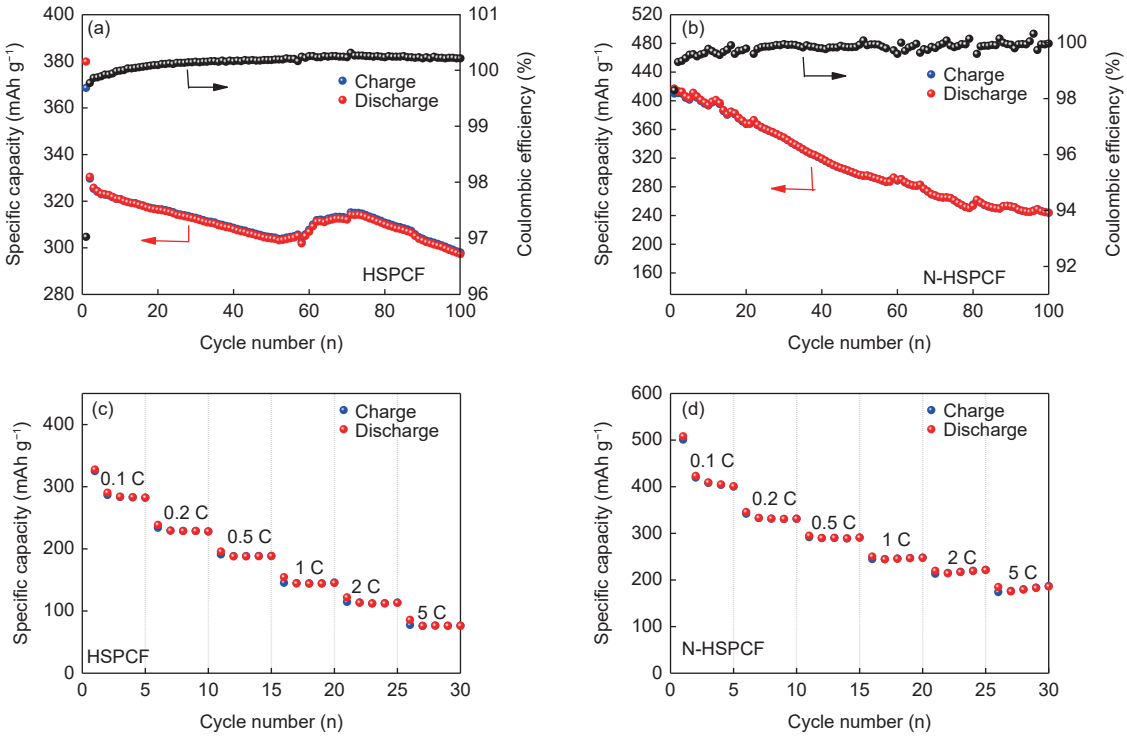

Fig. 9 Cycling performance, Coulombic efficiency and rate performance of (a,c) HSPCF/S electrodes and (b,d) N-HSPCF/S electrodes

N-HSPCF/S modified by hydrazine hydrate (Fig. 9b) increase to 420 mAh·g^{-1}. The result indicates that the increase of nitrogen content in HSPCF can improve the electrochemical performance. Because nitrogen doping can improve the fiber surface polarity, wettability, conductivity and adsorption capacity[31, 32]. Moreover, pyrrolic nitrogen and pyridine nitrogen have a relatively high electron cloud density, which can provide greater chemical bonding when combined with polysulfides, thus contributing to the enhancement of battery performance. The rate capability of HSPCF and N-HSPCF at different rates is presented in Fig. 9c, d. The current densities tested are from 0.1 to 2 C. The first discharge specific capacities of HSPCF electrodes at 0.1, 0.2, 0.5, 1, 2 and 5 C are 327.7, 234, 191, 145.5, 114.7 and 77.7 mAh·g^{-1}, respectively. The first discharge specific capacities of N-HSPCF electrodes at 0.1, 0.2, 0.5, 1, 2 and 5 C are 501, 342.1, 291.9, 244.8, 213.4 and 174.1 mAh·g^{-1}, respectively. The first specific capacities of N-HSPCF electrodes at different rate are significantly higher than those of HSPCF electrodes, which illustrates that HSPCF possesses better electrochemical performance.

The batteries with HSPCF and N-HSPCF are disassembled after 100 cycles. As shown in the insets of the Fig. 10, the PP separators of the HSPCF electrode possess yellow color, but the PP separators of the N-HSPCF electrode remain pale yellow, which is due to the shuttle effect. As illustrated in Fig. 10a, the HSPCF electrode surface are coated with block materials. In contrast, the surface of the N-HSPCF electrode is relatively clearer, implying the absence of massive materials observed in Fig. 10b.

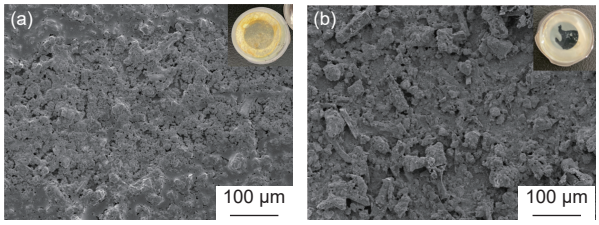

Fig. 10　SEM images of (a) HSPCF and (b) N-HSPCF electrode, insets of the cycled PP separators respectively

4　Conclusion

Nitrogen doped hollow-shaped porous carbon fiber (N-HSPCF/S) is successfully prepared by KOH activation and hydrazine hydrate modification using polyacrylonitrile as the precursor. It has a high specific surface area of 1 690 m^2·g^{-1} and nitrogen content of 8.81 at%. The abundant pore structures provide ample active sites and simultaenously, nitrogen doping improves the fibers' surface polarity, wettability, conductivity and adsorption capacity. Consequently, N-HSPCF/S shows good performance with an initial specific capacity of 420 mAh·g^{-1} at current density of 1 C when it is used as the electrode for the Li-S battery.

Acknowledgements

This work was supported by the Key Research and Development Program of Shanxi Province (202003D111002), the National Natural Science Foundation of China (51903249), the Innovation Fund Project of Shanxi Institute of Coal Chemistry, Chinese Academy of Sciences (SCJC-XCL-2022-12) and Major Science and Technology Special Plan of Shanxi Province (202101040201003).

References

[1] Zhong Y, Chao D, Deng S, et al. Confining sulfur in integrated composite scaffold with highly porous carbon fibers/vanadium nitride arrays for high - performance lithium –sulfur batteries[J]. Advanced Functional Materials, 2018, 28(38): 1706391.

[2] Kim J S, Hwang T H, Kim B G, et al. A lithium-sulfur battery with a high areal energy density[J]. Advanced Functional Materials, 2014, 24(34): 5359-5367.

[3] Zhou G, Li L, Ma C, et al. A graphene foam electrode with high sulfur loading for flexible and high energy Li-S batteries[J]. Nano Energy, 2015, 11: 356-365.

[4] You Y, Zeng W, Yin Y X, et al. Hierarchically micro/mesoporous activated graphene with a large surface area for high sulfur loading in Li-S batteries[J]. ournal of Materials Chemistry A, 2015, 3(9): 4799-4802.

[5] Miao L, Wang W, Yuan K, et al. A lithium-sulfur cathode with high sulfur loading and high capacity per area: a binder-free carbon fiber cloth-sulfur material[J]. Chemical communications, 2014, 50(87): 13231-13234.

[6] Fang R, Zhao S, Hou P, et al. 3D interconnected electrode materials

with ultrahigh areal sulfur loading for Li-S batteries[J]. Advanced materials, 2016, 28(17): 3374-3382.

[7] Chen K, Fang R, Lian Z, et al. An in-situ solidification strategy to block polysulfides in lithium-sulfur batteries[J]. Energy Storage Materials, 2021, 37: 224-232.

[8] Yang Y, Zheng G, Cui Y. Nanostructured sulfur cathodes[J]. Chemical Society Reviews, 2013, 42(7): 3018-3032.

[9] Pang Q, Liang X, Kwok C Y, et al. Advances in lithium-sulfur batteries based on multifunctional cathodes and electrolytes[J]. Nature Energy, 2016, 1(9): 1-11.

[10] Zheng G, Yang Y, Cha J J, et al. Hollow carbon nanofiber-encapsulated sulfur cathodes for high specific capacity rechargeable lithium batteries[J]. Nano Letters, 2011, 11(10): 4462-4467.

[11] Zhao M, Chen X, Li X Y, et al. An organodiselenide comediator to facilitate sulfur redox kinetics in lithium-sulfur batteries[J]. Advanced Materials, 2021, 33(13): 2007298.

[12] Feng X, Wang Q, Li R, et al. $CoFe_2O_4$ coated carbon fiber paper fabricated via a spray pyrolysis method for trapping lithium polysulfide in Li-S batteries[J]. Applied Surface Science, 2019, 478: 341-346.

[13] Ye J, He F, Nie J, et al. Sulfur/carbon nanocomposite-filled polyacrylonitrile nanofibers as a long life and high capacity cathode for lithium-sulfur batteries[J]. Journal of Materials Chemistry A, 2015, 3(14): 7406-7412.

[14] Cheng Z, Chen Y, Yang Y, et al. Metallic MoS_2 nanoflowers decorated graphene nanosheet catalytically boosts the volumetric capacity and cycle life of lithium–sulfur batteries[J]. Advanced Energy Materials, 2021, 11(12): 2003718.

[15] Park J H, Choi W Y, Yang J, et al. Nitrogen-rich hierarchical porous carbon paper for a free-standing cathode of lithium sulfur battery[J]. Carbon, 2021, 172: 624-636.

[16] Pang Z, Ma Y, Zhou Y, et al. Tailoring 3D carbon foam using CNTs and MnO_2 to fabricate stable lithium/dissolved lithium polysulfide batteries[J]. Langmuir, 2021, 37(13): 4016-4024.

[17] Zeng S, Arumugam G M, Liu X, et al. Encapsulation of Sulfur into N-doped porous carbon cages by a facile, template-free method for stable lithium-sulfur cathode[J]. Small, 2020, 16(39): 2001027.

[18] Singhal R, Chung S H, Manthiram A, et al. A free-standing carbon nanofiber interlayer for high-performance lithium-sulfur batteries[J]. Journal of Materials Chemistry A, 2015, 3(8): 4530-4538.

[19] Elazari R, Salitra G, Garsuch A, et al. Sulfur-impregnated activated carbon fiber cloth as a binder-free cathode for rechargeable Li-S batteries[J]. Advanced materials, 2011, 23(47): 5641-5644.

[20] Zhang J, Li Z, Lou X W. A freestanding selenium disulfide cathode based on cobalt disulfide-decorated multichannel carbon fibers with enhanced lithium storage performance[J]. Angewandte Chemie International Edition, 2017, 56(45): 14107-14112.

[21] Ryu Z, Zheng J, Wang M, et al. Nitrogen adsorption studies of PAN-based activated carbon fibers prepared by different activation methods[J]. Journal of colloid and interface science, 2000, 230(2): 312-319.

[22] Xiong L, Wang X F, Li L, et al. Nitrogen-enriched porous carbon fiber as a CO_2 adsorbent with superior CO_2 selectivity by air activation[J]. Energy & Fuels, 2019, 33(12): 12558-12567.

[23] Li L, Wang X F, Zhong J J, et al. Nitrogen-enriched porous polyacrylonitrile-based carbon fibers for CO_2 capture[J]. Industrial & Engineering Chemistry Research, 2018, 57(34): 11608-11616.

[24] Li Y, Lu C X, Zhang S C, et al. Nitrogen- and oxygen-enriched 3D hierarchical porous carbon fibers: synthesis and superior supercapacity[J]. Journal of Materials Chemistry A, 2015, 3(28): 14817-14825.

[25] Zhou C, Li X, Jiang H, et al. Pulverizing Fe_2O_3 nanoparticles for developing Fe_3C/N - codoped carbon nanoboxes with multiple polysulfide anchoring and converting activity in Li-S batteries[J]. Advanced Functional Materials, 2021, 31(18): 2011249.

[26] Chen P, Wu Z, Guo T, et al. Strong chemical interaction between lithium polysulfides and flame-retardant polyphosphazene for lithium-sulfur batteries with enhanced safety and electrochemical performance[J]. Advanced Materials, 2021, 33(9): 2007549.

[27] Yan S, Zhao M, Lei G, et al. Novel tetrazole-functionalized absorbent from polyacrylonitrile fiber for heavy-metal ion adsorption[J]. Journal of Applied Polymer Science, 2012, 125(1): 382-389.

[28] Pérez-Manríquez L, Aburabi'e J, Neelakanda P, et al. Cross-linked PAN-based thin-film composite membranes for non-aqueous nanofiltration[J]. Reactive and Functional Polymers, 2015, 86: 243-247.

[29] Chen D, Zhan W, Fu X, et al. High-conductivity 1T-MoS_2 catalysts anchored on a carbon fiber cloth for high-performance lithium-sulfur batteries[J]. Materials Chemistry Frontiers, 2021, 5(18): 6941-6950.

[30] Yang R, Li L, Chen D, et al. The enhancement of polysulfides adsorption for stable lithium-sulfur batteries cathode enabled by N-doped wrinkled graphene using solvothermal method[J]. ChemistrySelect, 2017, 2(35): 11697-11702.

[31] Zhu S, Wang Y, Jiang J, et al. Good low-temperature properties of nitrogen-ienriched porous carbon as sulfur hosts for high-performance Li-S batteries[J]. ACS Applied Materials & Interfaces, 2016, 8(27): 17253-17259.

[32] Wang Z, Niu X, Xiao J, et al. First principles prediction of nitrogen-doped carbon nanotubes as a high-performance cathode for Li–S batteries[J]. RSC Advances, 2013, 3(37): 16775-16780.

氮掺杂聚丙烯腈基中空炭纤维用于锂硫电池正极

牛静宜[1,2,4]，　经德齐[1,4]，　张兴华[1,4]，　苏维国[3]，　张寿春[1,2,4,*]

（1. 中国科学院 山西煤炭化学研究所 炭材料重点实验室，山西 太原 030001；
2. 中国科学院大学 材料与光电研究中心，北京 100049；
3. 海军工程大学 舰船综合动力系统国家重点实验室，湖北 武汉 430033；
4. 中国科学院碳纤维制备技术国家工程实验室，山西 太原 030001）

摘　要： 以聚丙烯腈（PAN）中空炭纤维为基体，通过 KOH 活化法制备了 PAN 中空多孔炭纤维用于锂硫电池正极材料基体。中空炭纤维经活化得到 2 491 $m^2 \cdot g^{-1}$ 的高比表面积和 1.22 $cm^3 \cdot g^{-1}$ 的大孔隙体积。为了进一步提高电化学性能，使用水合肼对纤维前体进行了改性，以制备氮掺杂的中空多孔炭纤维。修饰后的纤维拥有 1 690 $m^2 \cdot g^{-1}$ 的比表面积，0.84 $cm^3 \cdot g^{-1}$ 的孔隙体积和 8.81 at% 的高氮含量。由于含氮基团可以增加纤维表面极性和吸附能力，所以在电流密度为 1 C 时，其起始比容量可以提升至到 420 $mAh \cdot g^{-1}$。

关键词： 中空炭纤维；活化；改性；锂硫电池

中图分类号： TQ127.1$^+$1　　**文献标识码：** A

基金项目： 山西省重点研发计划资助项目 (202003D111002)；国家自然科学基金 (51903249)；2022 年度中国科学院山西煤炭化学研究所创新基金项目 (SCJC-XCL-2022-12)；山西省科技重大专项计划揭榜挂帅项目 (202101040201003).

通讯作者： 张寿春，研究员. E-mail: zschun@sxicc.ac.cn

作者简介： 牛静宜，硕士生. E-mail: niujingyii@163.com

本文的电子版全文由 Elsevier 出版社在 ScienceDirect 上出版（https://www.sciencedirect.com/journal/new-carbon-materials/）